

Capacity of Sun-driven Lunar Swingby Sequences and Their Application in Asteroid Retrieval

Hongru Chen¹(✉)

1. Department of Aeronautics and Astronautics, Kyushu University, Fukuoka, 8190395, Japan

✉ hongru.chen@hotmail.com

Received: 15 December 2022 / Accepted: 21 February 2023

Abstract

For deep-space mission design, the gravity of the Sun and the Moon can be first considered and utilized. Their gravity can provide the energy change for launching spacecraft and retrieving spacecraft as well as asteroids. Regarding an asteroid retrieval mission, it can lead to the mitigation of asteroid hazards and easy exploration and exploitation of the asteroid. This paper discusses the application of the Sun-driven lunar swingby sequence for asteroid missions. Characterizing the capacity of this technique is not only interesting in terms of dynamic insights but also non-trivial for trajectory design. This paper elucidates the capacity of a Sun-driven lunar swingby sequence with the help of the “Swingby-Jacobi” graph. The capacity can be represented by a range of Jacobi integral that encloses around 660 asteroids currently cataloged. To facilitate trajectory design, a database of Sun-perturbed Moon-to-Moon transfers, including multi-revolution cases is generated and employed. Massive trajectory options for spacecraft launch and asteroid capture can then be explored and optimized. Finally, a number of asteroid flyby, rendezvous, sample-return, and retrieval mission options enabled by the proposed technique are obtained.

Keywords

Asteroid mining · Planetary defense · Gravity assists · Asteroid flybys · Sample return · Moon-to-Moon transfers · Trajectory design · Reachable sets · Graphical methods

Nomenclature

NRHO	near-rectilinear halo orbit
SPMT	Sun-perturbed Moon-to-Moon transfer
GTO	geostationary transfer orbit
SE	Sun-Earth
CR3BP	circular-restricted three-body problem
GNC	guidance, navigation, and control operations
Δv	impulsive velocity increment
$\mathbf{v}_\infty, v_\infty$	vector and magnitude of the hyperbolic excess velocity with respect to a celestial body
M, E	subscripts indicating referencing to the Moon and the Earth, respectively
φ	swingby pump angle
δ	declination of the escape or incident trajectory
C_3	characteristic energy (also v_∞^2) with respect to the Earth
J	Jacobi integral in the SE-CR3BP
T_{oF}	time of flight
\mathcal{A}	reachable set with a Sun-driven lunar swingby sequence
\mathcal{A}_p	reachable set with a planar swingby sequence
\mathcal{B}	reachable domain of $v_{\infty E}$ and δ

1 Introduction

In space mission and trajectory design, gravity assists and low-energy transfers that take advantage of the gravity of celestial bodies are often considered for reducing fuel consumption as well as increasing the mass of payloads. For all the missions that depart from the Earth, the Moon is the closest celestial body that can provide a gravity assist. In fact, in the Sun-Earth-Moon system spacecraft is influenced by the joint gravitational effect from the Sun, the Earth, and the Moon. Trajectory design for missions such as the HITEN, ARTEMIS-THEMIS, NOZOMI, DESTINY, EQUULEUS, and Lunar Flashlight have employed

lunar swingbys driven by solar tides [1–7]. The joint gravitational effect can assist the launch of spacecraft and the capture of returning spacecraft as well as samples from the visited body. However, the joint gravitational effect has not been well characterized for mission analysis and trajectory design. This paper will clarify the capacity of a Sun-driven lunar swingby sequence and its application for asteroid retrieval.

Asteroids are considered to be promising bonanza that may contain water and rare metals. The resources can be used to sustain astronauts' lives, fuel spacecraft as well as power space bases. Developments on Earth can also benefit from asteroid mining. Furthermore, asteroids are of great scientific interest as they preserve pristine relics of the early solar system. Missions such as DAWN, NEAR, Hayabusa-1 and -2, and Osiris-REx have returned significant information and even samples that lead to a better understanding of asteroids and the solar system. An increasing number of missions, such as LUCY, PSYCHE, and MMX, will be visiting asteroids and asteroid-like small bodies. On the other hand, near-Earth asteroids (NEA) are threats to Earth for the constant possibility of Earth impacts. The Chelyabinsk meteor is an alert. It is time to “look up” and tackle potential asteroid attacks. NASA and ESA are working on the DART and HERA missions to demonstrate asteroid deflection technologies [8, 9]. In this context, the concept of asteroid retrieval has also been proposed. Asteroid retrieval is to bring an asteroid or a part of it to the vicinity of the Earth. That will not only mitigate the threat but also allows easy and constant visits to the asteroid. Moreover, the technology to retrieve asteroids becomes more realistic. For instance, retrieving an entire small NEA – approximately 7-m diameter with a mass of order 500,000 kg is believed to be possible by 2025 [10].

Several studies have investigated asteroid retrieval from the perspectives of propulsion technologies and trajectory design. This paper discusses the problem from the perspective of trajectory design. In this frame, the Sun-Earth libration-point dynamics has been proposed to capture asteroids [11–14]. As this method mostly relies on the natural capture by the gravity of the Sun and the Earth, it takes considerable time or Δv to retrieve a target. In addition, libration-point orbits are not stable. Constant station-keeping maneuvers are needed, which is not feasible in the long run. Without stationkeeping, the captured asteroid could become a serious hazard to Earth. The lunar swingby can change orbital energy more effectively. Landau et al. (2013) [15] and Gong and Li (2015) [16] proposed using lunar swingbys. Using this method, the v_∞ with respect to the Moon is considered invariable, and resulting orbits with their apogees beyond the Moon's orbit will be constantly influenced by the lunisolar perturbations, which are unstable and threatening to Earth. For stable capture, not only the characteristic energy with respect to the Earth should be minimized, but also v_∞ with respect to the

Moon. Urrutxua et al. (2015) [17] included the gravity of the Moon in the Sun-Earth Hill's problem, and ran extensive simulations to reveal temporary capture trajectories prolonged by tens to hundreds of m/s of Δv . Nevertheless, concrete characterization of the easily capturable orbit types (or objects) under the gravity of the Sun, the Earth, and the Moon, is still lacking.

The Sun-driven lunar swingby sequence investigated in this paper can change the v_∞ with respect to both the Earth and the Moon, and thus can be used for launching spacecraft and capturing the asteroid into a high lunar orbit or the Earth-Moon near-rectilinear halo orbit (NRHO), which is stable to the Earth. In this paper, the retrieval mission is considered through three phases. In the vicinity of the Earth, for the escape phase, a Sun-driven lunar swingby sequence is utilized to increase v_∞ of spacecraft with respect to the Earth, as well as target a certain direction for the asteroid. For the capture phase, a Sun-driven lunar swingby sequence is used to reduce the v_∞ of the asteroid with respect to the Moon to an acceptably low level, which allows inexpensive insertion to orbits stably confined to the Moon. In the heliocentric transfer phase, the spacecraft is sent to the targeted asteroid, and the asteroid is sent back to the Earth with permissible Δv . There are around 15000 NEA currently cataloged. Searching and optimizing possible heliocentric transfer and gravity-assisted trajectories are computationally expensive and time-consuming each time given an updated asteroid database. It is often desired to characterize the capacity (i.e., referred to as the reachable set, attainable set, or attractive set in literature) of certain trajectory design methods, for purposes of obtaining initial guesses, pruning search space, etc (e.g., Ref. [18–22]). For the problem of interest, characterizing the capacity of Sun-driven lunar swingby sequences for reaching and capturing heliocentric objects is not only interesting in terms of dynamical insights but also non-trivial for mission planning.

Graphical methods are sometimes helpful for trajectory design and analysis. Strange and Longuski (2002) [23] proposed the Tisserand graph with v_∞ contours for analyzing and deciding gravity-assist sequences. It is based on the patched two-body approximation. Poincaré map is useful in analyzing the three-body problem. Campagnola and Russell (2010) [24] further developed the Tisserand-Poincaré graph with the Tisserand (or Jacobi) contours that consider the third-body perturbation during swingby. Ross and Scheeres (2007) [25] proposed the periapsis-Poincaré map to analyze low-energy capture and escape. Those graphs are applicable for star-planets and planet-moons systems. For the star-planet-moon system concerned in this work, the Swingby-Jacobi graph developed by Chen et al. (2016) [5] and Chen (2017) [26] is applicable. In addition to the Jacobi integral in the Sun-Earth system, the effect of lunar swingby can also

be portrayed. The double Tisserand graph recently developed by Martens and Bucci (2022) [27] is notable and also applicable for the star-planet-moon system. The double Tisserand graph is suitable for analyzing transfers to the moon, while the Swingby-Jacobi graph is suitable for analyzing transfers to the heliocentric region. The Swingby-Jacobi graph is adopted in this paper to elucidate the accessibility of the Sun-driven lunar swingby sequence to the heliocentric region.

This paper is organized as follows. Sec. 2 presents the dynamic model used for the trajectory design and the mechanism of the sequence of Sun-perturbed Moon-to-Moon transfers (SPMT) and lunar swingbys for enhancing mission design. The Swingby-Jacobi graph is also introduced to visualize effects of Sun-perturbed transfers and lunar swingbys. Sec. 3 elucidates the capacity of a Sun-driven lunar swingby sequence with help of the Swingby-Jacobi graph. It is characterized by an accessible range of the Jacobi integral and accessible domain of the magnitude and declination of the v_∞ with respect to the Earth. These ranges effectively exclude the definitely inaccessible asteroids and inaccessible heliocentric transfer options among the optimized, the computation routine of which is presented in Sec. 4.1. To facilitate patching SPMT segments and lunar swingbys for meeting the escape or capture conditions, a database of SPMT solutions is established. The effort to compute the database is presented in Sec. 4.2.1. With the characterized capacity of this technique and the trajectory design tools, lists of the possible asteroid flyby, rendezvous, sample-return, and retrieval missions for the next 20 years are obtained, which are presented in Sec. 5. Disadvantages and advantages of the Moon-to-Moon transfer types, namely the short transfer, Sun-perturbed transfer, and three-dimensional transfer, are discussed in Sec. 6. Conclusions are given in the last section.

2 Dynamic Model and Swingby-Jacobi Graph

2.1 Dynamic Model

The motion of spacecraft and asteroid samples in the vicinity of the Earth is influenced by the gravity of the Sun, the Earth, and the Moon. To facilitate analysis and orbit design, the patched Sun-Earth circular restricted three-body problem (SE-CR3PB) and lunar swingby model is adopted. The synodic coordinate system, where the Sun-Earth barycenter is set at the origin, the Sun and Earth are fixed on the x-axis, and the

rotation direction is aligned with the z-axis, as shown in Fig. 1, is used. Let μ denote the ratio of the mass of the Earth to the total mass of the two bodies, the distance between the Sun and the Earth, AU, be the length unit, and the time unit is set in the way that the period of the Earth's becomes 2π . Then, equations of motion in the SE-CR3BP are expressed as,

$$\ddot{x} - 2\dot{y} = \partial U / \partial x \quad (1)$$

$$\ddot{y} + 2\dot{x} = \partial U / \partial y \quad (2)$$

$$\ddot{z} = \partial U / \partial z \quad (3)$$

where U denotes the pseudo-gravitational potential expressed as,

$$U = (x^2 + y^2)/2 + (1 - \mu)/r_1 + \mu/r_2 \quad (4)$$

where $\mu = 3.0035 \times 10^{-6}$ for the Sun-Earth system, and the distances,

$$r_1 = \sqrt{(x + \mu)^2 + y^2 + z^2}, \quad r_2 = \sqrt{(x - 1 + \mu)^2 + y^2 + z^2} \quad (5)$$

An energy quantity, known as the Jacobi integral, holds in the CR3BP system. The Jacobi integral J is expressed as,

$$J = (\dot{x}^2 + \dot{y}^2 + \dot{z}^2) - 2U \quad (6)$$

Trajectories are considered in the SE-CR3BP most of the time. The lunar gravity is approximated by the lunar swingby only effective at a lunar encounter. In other words, the object gets an instantaneous velocity change (i.e., \mathbf{v}_∞ with respect to the Moon gets an instantaneous bend) at the lunar encounter. The inclination and eccentricity of the Moon's orbit are small and are set to zero in this simplified model. Such a SE-CR3BP plus lunar swingby model is schematically depicted in Fig. 1.

2.2 Sun-perturbed Moon-to-Moon transfers

For a trajectory seen as an Earth orbit, the v_∞ with respect to the Moon, $v_{\infty\mathbf{M}}$, remains constant, if solar gravity is not taken into account. In the presence of solar perturbations, $v_{\infty\mathbf{M}}$ will be changed as the "Earth" orbit reaches a far region where solar perturbations are significant. To illustrate, Fig. 2 schematically depicts the solar tidal force in the Earth-centered inertial frame and its effect on orbits around the Earth. As shown, after the first lunar swingby (S1), or an outward crossing of the Moon's orbit, the resulting orbit with its

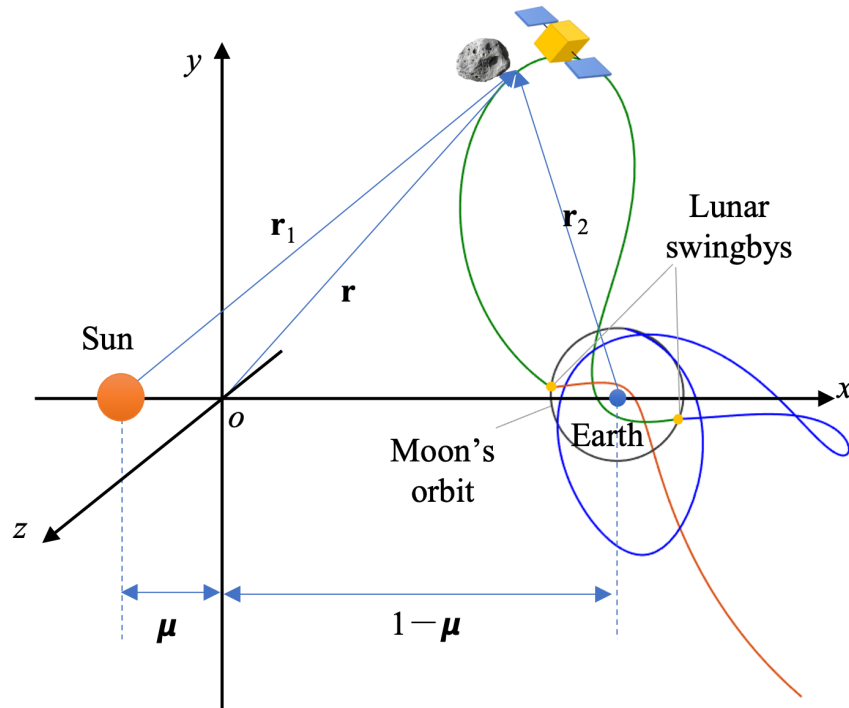


Fig. 1 Schematic of the patched Sun-Earth CR3BP and lunar swingby model.

apogee far away in the 1st or 3rd quadrants will experience posigrade deceleration near the apogee, and come back to a second lunar swingby (S2) with a larger encounter angle α with respect to the Moon's orbit, and can even be in a retrograde direction. Even though the velocity is decreased (considering the posigrade situation), $v_{\infty M}$ is still increased because of the increased α . This mechanism is further clarified via the Swingby-Jacobi graph introduced in the next section. In contrast, an orbit with its apogee in the 2nd or 4th quadrants will be accelerated, resulting in a decreased $v_{\infty M}$ at S2 or missing the Moon's orbit. Such Sun-perturbed Moon-to-Moon transfers (hereafter referred to as the SPMT or Sun-perturbed M-M transfers) can be employed to improve the lunar encounter condition for a gravity-assisted escape, as planned for the NOZOMI and DESTINY missions [3–5], or for an inexpensive insertion into a lunar orbit, as applied in the HITEN, ARTEMIS-THEMIS, EQUULEUS, and Lunar Flashlight missions [1, 2, 6, 7].

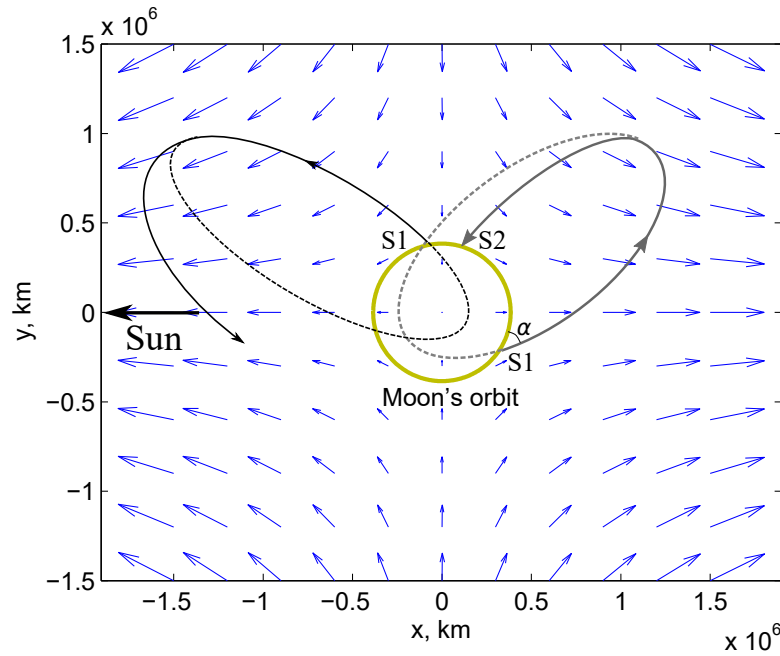


Fig. 2 The solar gravitational influence on orbit states with respect to the Earth and the Moon (figure reused from Ref. [5, 26]).

2.3 Swingby-Jacobi graph

Given $v_{\infty M}$ and the pump angle φ (i.e., angle between the $\mathbf{v}_{\infty M}$ and Moon's velocity \mathbf{v}_M vectors) one can compute the Jacobi integral J in the SE-CR3BP. Although J can vary with the position of the lunar encounter and the out-of-plane degree of $\mathbf{v}_{\infty M}$, these factors only vary Jacobi integral within an insignificant range. Figure 3 plots contours of J on the $v_{\infty M}$ - φ plane. In this graph, a lunar swingby can be portrayed by the vertical motion of a state (blue dot), which changes J in the Sun-Earth system. The following M-M transfer can be perturbed by the Sun, while J is maintained. The solar perturbation can be portrayed by the motion along the Jacobi contour. The Jacobi contours and the $v_{\infty M}$ - φ plane constitute the basis of the “Swingby-Jacobi” graph. Orbital information can be added to this graph, which enables insights into the orbit dynamics and effects on the mission. Figure 3 includes contours of the encounter angle α and osculating (i.e., at the lunar encounter) characteristic energy C_3 (i.e., v_{∞}^2) with respect to the Earth. It can be seen that in the direction that C_3 is decreased and α is increased, which corresponds to the situation of posigrade deceleration in the 1st and 3rd quadrants (or the retrograde deceleration in the 2nd and 4th quadrants), $v_{\infty M}$ is increased. This

visualizes and explains the mechanism by which $v_{\infty M}$ increases while C_3 decreases during a Sun-perturbed transfer. To conclude, the following situations are visualized in the graph.

- The orbital energy w.r.t. the Earth, represented by C_3 , is influenced by lunisolar perturbations;
- The Jacobi integral in the Sun-Earth three-body problem, represented by J , is influenced by lunar gravity;
- The orbital energy w.r.t. the Moon, represented by $v_{\infty M}$, is influenced by solar gravity;
- $v_{\infty M}$ is increased as C_3 is decreased (and vice versa) during a Sun-perturbed transfer.

Therefore, a sequence of Sun-perturbed M-M transfers and lunar swingbys can be utilized to 1) assist Earth escape and asteroid encounter, which is to achieve certain C_3 , J , and escape direction, and 2) asteroid capture, which is to reduce $v_{\infty M}$ for inexpensive lunar orbit insertion. Other information can also be added to this graph. For instance, the maximum post-swingby C_3 is also a function of the pre-swingby φ and $v_{\infty M}$, and thus can be plotted in the Swingby-Jacobi graph. Given an initial state, the achievable C_3 after two swingbys can be revealed, which is presented in Ref. [5]. Characterization of the capacity of a Sun-driven lunar swingby sequence in Sec. 3.1 is aided by this graph.

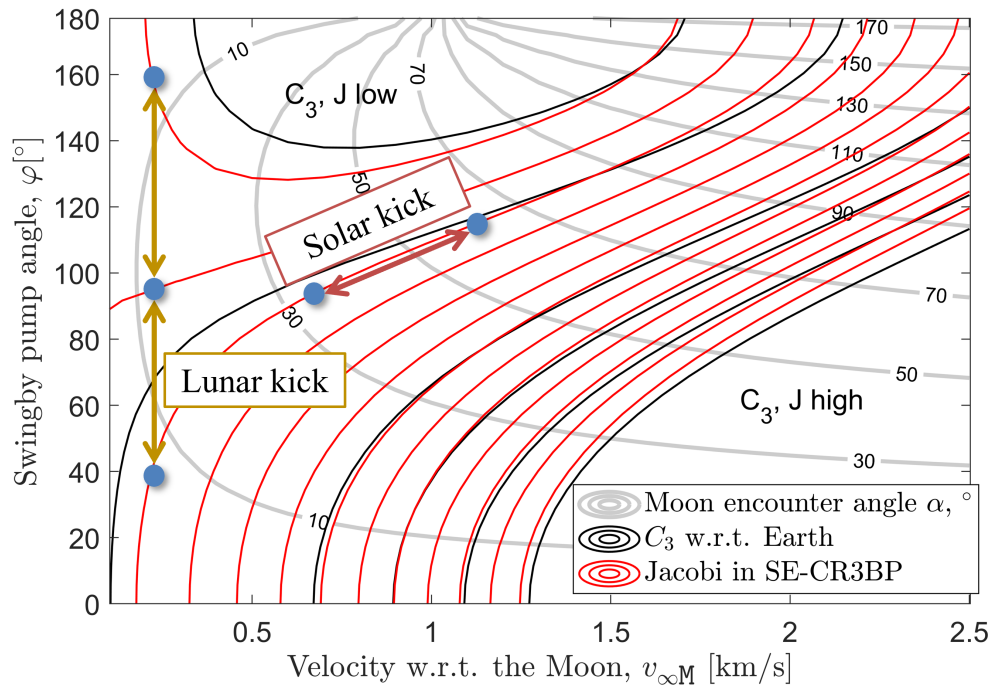


Fig. 3 Swingby-Jacobi graph

2.4 Trajectory design objectives

It can therefore be expected to launch spacecraft with a low initial $v_{\infty M}$ to deep space, and to reduce the $v_{\infty M}$ of returned spacecraft and asteroid samples for an inexpensive insertion to a stable lunar orbit, using the Sun-driven lunar swingby sequence. The low-cost initial $v_{\infty M}$ (i.e., before acceleration via a Sun-driven lunar swingby sequence) is commonly between 200 m/s (i.e., for a direct transfer from a GTO) and 800 m/s (i.e., via the low-thrust spiral orbit raising). Therefore, for the Earth escape that targets an asteroid, the objective of trajectory design is to minimize the initial $v_{\infty M}$ to below 800 m/s. For spacecraft and asteroid capture, the objective is to achieve a final $v_{\infty M}$ smaller than 450 m/s, enabling insertion into a mid- to high-lunar orbit at a Δv of around 350 m/s or a stable NRHO at 20 m/s [7, 28, 29]. Another propulsion system launched years later to the Earth-Moon regime can possibly provide this insertion Δv can while waiting to dock with the returned spacecraft and asteroid.

3 Capacity of Sun-driven lunar swingby sequences

There are around 15,000 cataloged near-Earth asteroids. Each has hundreds of locally optimal heliocentric transfer trajectories from and to the Earth's vicinity given an interval of 20 years. Each Earth escape or Earth encounter condition leads to hundreds to thousands of possible lunar swingby sequences given the computed database of SPMT (introduced in Sec. 4.2.1) and a limit of two SPMT segments. Computing all of the possible trajectories each time the asteroid database is updated can be very time-consuming. Therefore, it is desired to reduce the search space with the capacity of a Sun-driven lunar swingby sequence characterized.

3.1 Accessible energy range

Looking at the Swingby-Jacobi graph, it may seem that an orbit state can be smoothly moved between the left side (i.e., small $v_{\infty M}$) and the right side (i.e., large $v_{\infty M}$). However, as $v_{\infty M}$ increases, the bending angle of $\mathbf{v}_{\infty M}$ becomes more further restricted, and so does the Jacobi jump. When $v_{\infty M}$ is large (i.e., > 2.5 km/s), it can take many segments of SPMT and lunar swingby to substantially reduce or increase $v_{\infty M}$. Additionally, when $v_{\infty M}$ is large, C_3 with respect to the Earth is inevitably large, and the SPMT is in a hyperbolic arc whose ToF is generally longer than 200 days. Therefore, using the Sun-driven lunar swingby sequence is not efficient when C_3 and $v_{\infty M}$ are large.

Time is a critical factor for space missions. In this work, the ToF of an M-M transfer is limited to 200 days, and the number of patched SPMTs is limited to 2. The ToF constraint essentially restricts the maximum accessible C_3 . Among all the SPMT limited by 200 days, which have been solved for the database, C_3 is generally below 0 (although a few solutions reach $0.7 \text{ km}^2/\text{s}^2$). Therefore, a constraint is applied that limits C_3 to 0 before the last (or after the first) lunar swingby for escape (or capture) purposes. Additionally, the limit of bending angle γ of $\mathbf{v}_{\infty M}$ at the lunar swingby constrains the maximum pre-swingby or post-swingby C_3 , $C_{3 \max}$. γ is limited by [30],

$$\gamma_{\max} = \pi - 2 \times \arccos \left[G_M / (G_M + r_{\min} \cdot v_{\infty M}^2) \right] \quad (7)$$

where G_M is the gravitational parameter of the Moon and r_{\min} is the minimum flyby radius, which is set to 1838 km (i.e., 100 km above the surface of the Moon). This constraint also restricts the capacity of a Sun-driven lunar swingby sequence.

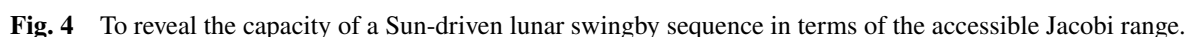
To express the effects of those constraints, the $C_3 = 0$ contour is highlighted on the Swingby-Jacobi graph as shown in Fig. 4. For $C_3 = 0$, the corresponding φ that leads to the maximum pre-swingby or post-swingby C_3 while constrained by γ_{\max} is plotted as a blue line on the graph. The area bounded by these two lines indicates the accessible heliocentric orbit states after or before a Sun-driven lunar swingby sequence. The maximum accessible J is obtained at the tangent point (annotated by a circle in Fig. 4) of the $C_{3 \max}$ boundary (blue) and the Jacobi contours, which is -2.9965. The loosely equivalent C_3 is $3.3 \text{ km}^2/\text{s}^2$, and the v_{∞} with respect to the Earth, $v_{\infty E}$, is 1.8 km/s. In addition, orbits of low J may pass by the Earth through the Sun-Earth Lagrangian L_1 point, where $J = -3.0009$. The accessible J indicates the accessible heliocentric orbits, as the Jacobi integral can be expressed in the Tisserand form as a function of orbital elements (for details, see Ref. [31]), which is,

$$J = -(1 - \mu)/a - 2\sqrt{a(1 - \mu)(1 - e^2)} \times \cos i \quad (8)$$

where a , i , and e are the semi-major axis, inclination, and eccentricity of a heliocentric orbit, respectively. The reachable set \mathcal{A} with a Sun-driven lunar swingby sequence can be expressed as,

$$\mathcal{A} \supset \{(a, e, i) | -3.0009 < J < -2.9965\} \quad (9)$$

The superset above means there is another situation that can further expand the accessible heliocentric region. McElrath et al. (2012) [32] discussed the application of the retrograde inner M-M transfer. This kind



of transfer is short (i.e., 4 to 15 days) and inside the Moon's orbit, and thus is not considered a Sun-perturbed transfer. The $v_{\infty M}$ is thus the same at the two consecutive lunar encounters. Some of these transfers are hyperbolic arcs. To illustrate its useful features for the problem of interest, the solutions of inner transfers are manifested as a green curve with ends in Fig. 4. The lower end are associated with the minimum Earth flyby altitude, which is 220 km in this work. The orbit state can be considered to jump vertically twice as a result of the two consecutive lunar swingbys of this transfer. Therefore, boundaries of the φ leading to and resulting from the swingbys of the inner M-M transfers are also plotted in Fig. 4. The orbit state above the lower φ boundary (cyan) can be transferred from or to a state with $C_3 < 0$ with two lunar swingbys of the short inner transfer. Therefore, this kind of transfer provides another accessible area in the heliocentric region, which is a triangle-like area outside the aforementioned blue boundary. It can be read out that the accessible J is up to -2.9946, loosely equivalent to a C_3 of 4.83 km²/s² and a $v_{\infty E}$ of 2.2 km/s. However, the distribution of

this level of J is not isotropic in space. The reason is that the inner M-M transfer requires bending the escape (or incident) trajectory from (or onto) the ecliptic plane, and the constraint of bending angle increases with velocity. This will be further analyzed in the next subsection. Then, the reachable set is a subset expressed as,

$$\mathcal{A} \subset \{(a, e, i) | -3.0009 < J < -2.9946\} \quad (10)$$

3.2 Accessible direction range

To use the inner M-M transfer, it should be connecting the lunar swingby sequence and the heliocentric trajectory, namely, as the last segment of the escape phase, or the first segment of the capture phase. This requires the last (or the first) swingby to bend the $\mathbf{v}_{\infty M}$ from (or onto) the ecliptic plane given the targeted escape (or incident) \mathbf{v}_{∞} with respect to the Earth, $\mathbf{v}_{\infty E}$, which may not be in the plane.

If only SPMTs are employed, it is also preferred to bend the last (or first) $\mathbf{v}_{\infty M}$ from (or onto) the plane to perform a planar Sun-driven lunar swingby sequence. As reasoned in Sec. 6.2, three-dimensional SPMTs do not result in significant change in $v_{\infty M}$ and thus are not efficient given the constraint on ToF and number of SPMTs. Because of the bending angle constraint, the escape (or capture) condition becomes more difficult to achieve as the targeted declination of $\mathbf{v}_{\infty E}$ increases. It is thus necessary to derive the relationship between the accessible ranges of the magnitude $v_{\infty E}$ and declination δ of $\mathbf{v}_{\infty E}$.

The escape and incident $\mathbf{v}_{\infty E}$ can be related to an Earth orbit. Note that the solar perturbation is not considered for the escape and incident arc (i.e., connecting the heliocentric phase and swingby phase), because of the short effect and the sake of simplicity. The corresponding Earth orbit has an inclination ranging from δ to 90° . The inclination is determined by the difference between the ascension of $\mathbf{v}_{\infty E}$ and the lunar phase at the lunar encounter. For the same $v_{\infty E}$ and thus the same velocity at the lunar encounter, and the same $v_{\infty M}$, a low-inclination orbit results in lower declination of $\mathbf{v}_{\infty M}$ than a high-inclination orbit (see the illustration in Fig. 5). It is more difficult to bend the $\mathbf{v}_{\infty M}$ of higher declination from (or onto) the plane.

To exam the accessible situation for an escape (incident) vector of certain $v_{\infty E}$ and δ , one can vary the lunar encounter position, compute the orbit state at the encounter (i.e., applying Appendix) and the bending angle limit (Eq. 7), and examine whether the orbit state at the encounter can be bent from (or to) the ecliptic plane with $C_3 < 0$. By examining various lunar encounter phase, $v_{\infty E}$, and δ , a two-dimensional accessible area in Fig. 6, is revealed. In addition, the situation with one inner M-M transfer in the sequence is considered. The

judgment for this situation is whether the state can be bent from (or to) the solution of the inner transfer (i.e., depicted by the green line in Fig. 4). The corresponding boundary is also shown in Fig. 6. Let the combined accessible domain in Fig. 6 be denoted by a set \mathcal{B} . The reachable set with a planar Sun-driven lunar swingby sequence, \mathcal{A}_p , can be expressed as,

$$\mathcal{A}_p = \{(a, e, i) | (v_{\infty E}, \delta) \in \mathcal{B}\} \quad (11)$$

While the orbital elements can be loosely mapped from $v_{\infty E}$ and δ , because \mathcal{B} cannot be expressed as a single function, characterizing Eq. 11 into explicit functions is not specifically performed in this work. Instead, Eq. 10 is used to pre-select potential candidates, and Eq. 11 is used in a later step to verify the true accessibility, as is demonstrated in Sec. 5.

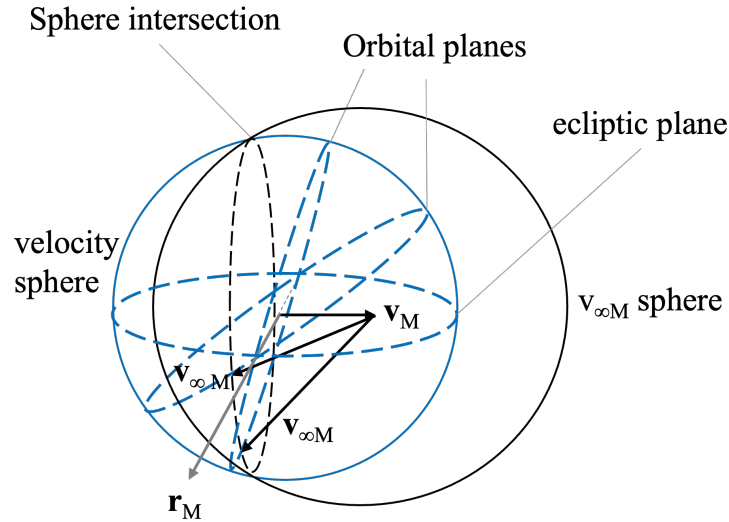


Fig. 5 Lunar encounter situations for specified velocity and $v_{\infty M}$.

Fig. 6 also shows that a Sun-driven lunar swingby sequence (constrained by ToF and number of SPMTs) can at least achieve or absorb a $v_{\infty E}$ up to 1.46 km/s in all directions. The corresponding C_3 is $2.13 \text{ km}^2/\text{s}^2$, and the loosely equivalent J is -2.9980. Thus, \mathcal{A}_p contains the subset associated with this Jacobi range, which is expressed as,

$$\mathcal{A}_p \supset \{(a, e, i) | -3.0009 < J < -2.9980\} \quad (12)$$

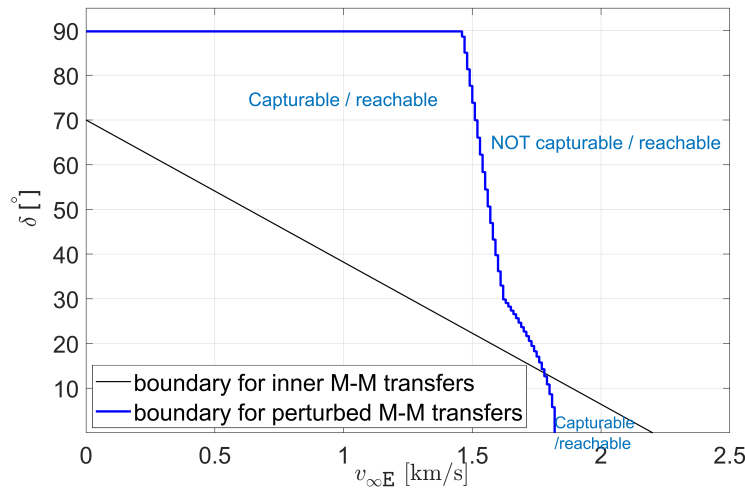


Fig. 6 Accessible domain of the $v_{\infty E}$ magnitude and its declination.

3.3 Potentially accessible asteroids

Because spacecraft do not generally rendezvous with an asteroid, a Δv to stop it at the asteroid, denoted by Δv_{stop} , is required. Similarly, an asteroid does not commonly reach the Earth's vicinity without a Δv to return it, denoted by Δv_{retn} . Nevertheless, asteroids whose orbits are outside the reachable set cannot be reached or returned with a small Δv to cancel the expected large velocity difference at the intersection. The characterized capacity of a Sun-driven lunar swingby sequence also indicates easily accessible targets. To show the increased capacity with the proposed method, a comparison to the methods using lunar swingbys and the Sun-Earth libration dynamics on the accessible Jacobi and the corresponding number of potential targets in the current asteroid database is presented in Table 1.

Δv_{stop} and Δv_{retn} are limited to a small amount, such that the effect of gravity assists is still dominant and we do not depart away from the idea of easily reachable and retrievable asteroids. For reaching the target, a Δv_{stop} budget of 1 km/s is assumed available. For retrieving spacecraft and samples from the target, a Δv_{retn} budget of 500 m/s is assumed available. These Δv budgets can also enable low energy asteroids to reach Sun-Earth L_1 and pass by the Earth, and thus alter the lower bound of the accessible Jacobi range. After subtracting the kinetic energy attributed to the Δv budget from the J at L_1 , the lower bound of the J of the reachable asteroid becomes -3.0020, and that of the retrievable becomes -3.0012. These Jacobi ranges are applied in the first place to exclude the definitely inaccessible asteroids.

Table 1 Comparison of different gravity-assist methods

Method		Accessible Jacobi	Number of candidates ^d
Lunar swingbys		$[-3.0009, -2.9962]$ ^a	491
S-E libration-point dynamics		$[-3.0009, -2.9992]$ ^b	168
Sun-driven lunar swingby sequence	only SPMTs	$[-3.0009, -2.9965]$ ^c	456
	with an inner transfer	$[-3.0009, -2.9946]$ ^c	657

^a Gong and Li (2015) [16]

^b Sanchez and Garcia Yarnoz (2016) [14]

^c The present work and Chen (2017) [26]

^d Based on the database of the Minor Planet Center: <https://minorplanetcenter.net/iau/MPCORB/MPCORB.DAT>, accessed on 2022 Aug. 15.

4 Trajectory design

4.1 Heliocentric transfer phase

As a Sun-driven lunar swingby sequence can reach or absorb a $v_{\infty E}$ of 1.46 km/s at the least (see Fig. 6), and the heliocentric transfer Δv_{stop} and Δv_{retn} provided by propulsion systems are limited to 1 km/s and 500 m/s, respectively, minimizing the Δv cost in the heliocentric transfer phase is crucial. A Lambert solver for the two-body problem and the Matlab Fmincon routine are used to find low- Δv transfer trajectories between the Earth and asteroids. The free variables, $\Delta \mathbf{v}$ vector, and epochs of Earth departure, asteroid arrival, asteroid departure, and Earth arrival, are optimized. The Lambert solver can consider multiple revolutions and return multiple solutions. In this work, up to three revolutions of heliocentric transfer are considered. However, the Lambert solver is not called in the optimization routine but is only used to provide initial guesses of $\Delta \mathbf{v}$. Starting with the initial guess, the Fmincon routine can continue to compute the optimal trajectory with the fed gradients whose expressions are available in Ref. [33], pg. 467. Furthermore, using the numerical optimization routine to solve the two-point boundary problem can avoid the singularity problem in the Lambert solver when the revolution number jumps. Once an optimal transfer trajectory with $\Delta v_{\text{stop}} < 1$ km/s (or $\Delta v_{\text{retn}} < 500$ m/s) is found, the corresponding escape (or incident) condition, $\mathbf{v}_{\infty E}$ as well as its declination δ , is known, and the accessible domain described in Sec. 3.2 can be applied to exclude the impossible transfer trajectories.

4.2 Escape and capture phases

The escape (or capture) phase involves a sequence of Moon-to-Moon transfers and lunar swingbys to reduce the initial (or final) $v_{\infty M}$ to < 800 m/s (or 450 m/s), given the targeted escape (or incident) $\mathbf{v}_{\infty E}$ connected with the heliocentric transfer phase. In addition, the number of SPMT segments is preferred to be minimal, not only to limit the total flight time but also to minimize the operational risk. This work limits the number of SPMT segments to 2.

Given an escape (or incident) $\mathbf{v}_{\infty E}$, different lunar encounter positions result in different $\mathbf{v}_{\infty M}$ (see Appendix) and thus affect the sequence of lunar swingbys. The first (or final) lunar encounter position depends on the phase angle θ (i.e., defined by the angle of the Earth-to-Moon direction from the Sun-to-Earth direction in this work). Strictly speaking, θ depends on the departure (or arrival) date and the ephemeris of the Moon. However, as the ToF of the heliocentric phase (i.e., 250 to 1500 days) is much longer than the synodic period of the Moon (i.e., 30 days), it is assumed that a small Δv can vary the departure (or arrival) date by 15 days without significantly affecting $\mathbf{v}_{\infty E}$. Therefore, θ is considered a variable in the exploration of lunar swingby sequences. This will allow more options for lunar swingby sequences as well as more chance of meeting the $v_{\infty M}$ objective. To facilitate patching SPMT segments and lunar swingbys, a database of SPMT solutions is used. The following subsection presents the steps for generating this database.

4.2.1 Database of Sun-perturbed Moon-Moon Transfers

With significant solar perturbations, the Sun-perturbed Moon-Moon Transfer (SPMT) cannot be solved analytically. Nevertheless, the condition of SPMT can be defined by only two variables: θ and $v_{\infty M}$, which are practically bounded. $v_{\infty M}$ is bounded as the ToF of an M-M transfer is limited to an acceptable time. Therefore, the grid search method is applicable [34]. The solution of SMPT includes two variables: the post-swingby direction angle ψ of the post-swingby $\mathbf{v}_{\infty M}^+$, and the ToF for lunar re-encounter. Lantoine and McElrath (2014) [34] have classified the SMPT into families according to the ToF range and whether the beginning and the end of the transfer trajectory go in (i.e., noted by “i”) or out (i.e., noted by “o”) of the Moon’s orbit. The M-M transfers of the same family exhibit continuation on θ , $v_{\infty M}$, ψ , and ToF . Therefore, solutions of a family can be recovered if one solution of the family has been obtained. Furthermore, García Yárnoz et al. (2016) [6] used the analytical expression of the gradient of the solution space to generate initial

guesses for the neighboring grid nodes. However, they also noted that as ToF increases, the classification of families becomes complicated. Moreover, singularity happens as the perigee of the solution reaches a small value. Thus, it is tricky to determine the profile of families in the solution space. Without full knowledge, the continuation method is likely to miss solutions.

Considering that the database of SPMT, once established, can be accessed repeatedly, the computation time to compute such a database is not a primary concern. Therefore, despite its tediousness, the following effort has been made to ensure the completeness of the database. Solutions for every grid node defined by θ and $v_{\infty M}$ are computed regardless of the classification of the family. However, there are infinite solutions if ToF is not limited. In this work, ToF is limited to 200 days. In addition, when $v_{\infty M}$ is smaller than 0.4 km/s, the gravity loss becomes significant and the model of patching M-M transfers in the SE-CR3BP cannot hold very true. When $v_{\infty M}$ is greater than 2.2 km/s, the trajectory is mostly hyperbolic and cannot come back to the Moon in 200 days. Therefore, mesh grid is generated by sampling $v_{\infty M}$ from 0.4 to 2.2 km/s spaced by 0.1 km/s and θ from 0° to 360° spaced by 2° . To solve for the SPMT for a given grid node, a combination of adaptable-step search on ψ and differential correction on ψ and ToF is used (see Ref.[26] for details). A constraint that the perigee must be greater than 6600 km for the transfer trajectories is applied. In addition, multiple-revolution (multi-rev) transfers can also be computed with this method. The options of lunar swingby sequences are greatly expanded by including multi-rev solutions. Figure 7 presents example SPMT with initial $v_{\infty M} = 1.2$ km/s. They are grouped into the families defined by Lantoine and McElrath (2014) [34], where the resonance $p : q$ indicates the transfer trajectory makes p revolutions (i.e., defined by the number of apogees) while the Moon rotates q revolutions. Changes in lunar encounter situations at the ends of the Sun-perturbed transfers can be clearly seen.

On the other hand, the solution space where the SPMT encounters the Moon tangentially and where ToF is long is highly nonlinear, and therefore the computation is very sensitive to the initial guess. There are solutions missed in the previous step. Thus, in the second step, a scan is performed. To be specific, the continuation method is used to generate solutions for neighboring grid nodes based on every existent solution. When a new solution is found, it is added to the database. With all these efforts, the computed database is believed to be almost complete.

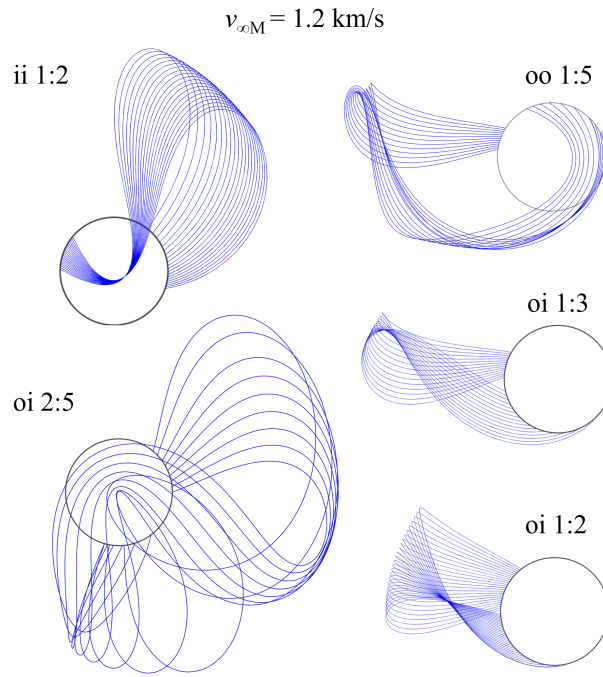


Fig. 7 Example Sun-perturbed Moon-to-Moon transfers (synodic frame).

5 Results

Fig. 8 summarizes the workflow for finding retrievable asteroids and the possible mission and trajectory profiles, where filters defined by the reachable sets, namely, accessible Jacobi range and $\mathbf{v}_{\infty E}$ domain, are applied. The workflow for asteroid rendezvous is similar to that in Fig. 8 and is thus not presented. Some of the candidates enclosed by the accessible Jacobi range may be found inaccessible for the given interval (e.g., 2023-2043 used in this work) because of the unachievable escape (or incident) condition, or no sequence of lunar swingbys found to meet the initial (or final) $v_{\infty M}$ requirement. Nevertheless, a number of accessible asteroids and feasible mission options are found.

Table 2 summarizes the 48 asteroids that spacecraft can rendezvous with before 2043. Each asteroid can be reached with a Sun-driven lunar swingby sequence and a $\Delta v_{\text{stop}} < 1$ km/s. The orbital elements, the number of observations n_{obs} , number of oppositions, n_{opp} , absolute magnitude, H , suspected diameter, D , and orbit class of the asteroids are also listed for the reference of mission planners. Note that for each listed asteroid, there could be one to hundreds of heliocentric transfer options whose escape condition can be met by at least one option of Sun-driven lunar swingby sequence. Not all feasible mission profiles can be presented in this

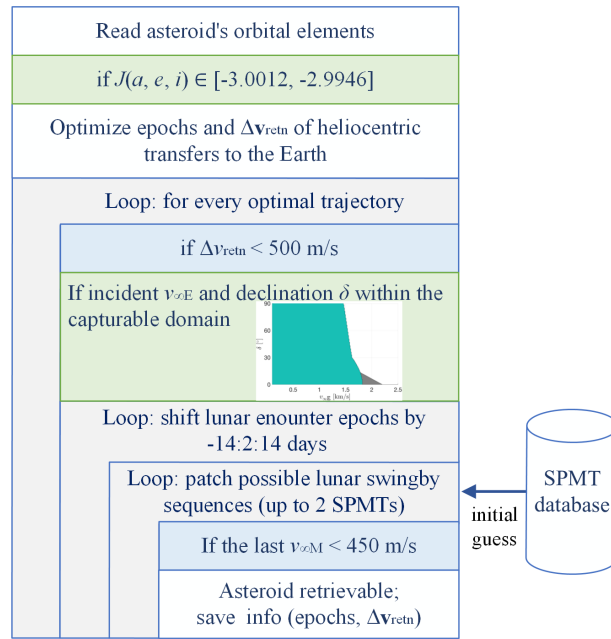


Fig. 8 The workflow to find retrievable asteroids and feasible trajectory options considering the capacity of a Sun-driven lunar swingby sequence (green blocks).

paper, but the missions prioritizing the flight time TOF and the asteroid observation time T_{obs} are selected to present in Table 3. T_{obs} represents the minimum time to observe the asteroid if the required Δv_{stop} cannot be fully paid. It is related to H , the velocity vector of spacecraft with respect to the asteroid, and the camera detection magnitude [35]. This work adopts the camera magnitude of 12, which was used by the low-cost micro-probe PROCYON [36]. As the table indicates, even without Δv_{stop} , the Sun-driven lunar swingby sequence still can permit asteroid flybys to closely observe asteroids for hours to more than one week (e.g., for 1991 VG, 2000 SG344, 2014 YD, 2017 TB18, and 2017 BN93).

Table 2 Easily reachable asteroids before 2043

Asteroid Des. ID	H	i [°]	e	a [AU]	D [m]	n_{obs}	n_{opp}	Class
1991 VG	28.3	1.4	0.052	1.032	10	66	3	Apollo
2000 LG6	29.0	2.8	0.111	0.917	7	13	1	Aten
2000 SG344	24.7	0.1	0.067	0.977	37	31	2	Aten
2001 GP2	26.4	1.3	0.072	1.035	25	58	2	Apollo
2005 QP87	27.7	0.3	0.175	1.233	10-15	85	1	Amor

2006 RH120	29.5	0.6	0.024	1.033	6	133	2	Apollo
2006 UB17	26.3	2.0	0.103	1.140	15-33	28	1	Amor
2007 UN12	28.7	0.2	0.059	1.049	9	132	2	Apollo
2007 VU6	26.5	1.2	0.091	0.976	13-29	38	1	Aten
2008 EA9	27.7	0.4	0.075	1.050	14	56	1	Apollo
2008 HU4	28.3	1.4	0.056	1.071	7	77	2	Amor
2008 UA202	29.4	0.3	0.068	1.033	5	16	1	Apollo
2009 BD	28.1	1.3	0.051	1.062	10	178	3	Apollo
2009 YR	28.0	0.7	0.110	0.942	12	29	1	Aten
2010 JW34	28.1	2.3	0.055	0.981	12	55	1	Aten
2010 UJ	26.2	0.4	0.092	0.950	20	12	1	Aten
2010 UE51	28.3	0.6	0.060	1.055	7	175	1	Apollo
2010 VQ98	28.2	1.5	0.027	1.023	11	49	1	Apollo
2011 BL45	27.1	3.1	0.021	1.038	18	24	1	Apollo
2011 BQ50	28.0	0.4	0.098	0.950	7-15	25	1	Amor
2011 MD	28.0	2.5	0.037	1.056	5.19	1487	1	Amor/Apollo
2011 UD21	28.5	1.1	0.030	0.979	10	83	1	Aten
2012 TF79	27.4	1.0	0.038	1.050	16	63	1	Apollo
2012 WR10	28.7	0.3	0.112	1.085	9	42	1	Apollo
2013 BS45	25.9	0.8	0.084	0.992	31	92	2	Aten
2013 EC20	29.0	1.3	0.121	1.113	7	55	1	Apollo
2013 RZ53	31.1	2.1	0.028	1.017	2	31	1	Apollo
2014 DJ80	26.3	3.0	0.067	0.977	27	30	1	Aten
2014 HN2	26.3	1.2	0.118	0.927	26	65	1	Aten
2014 QN266	26.3	0.5	0.092	1.053	27	82	1	Apollo
2014 UV210	26.9	0.6	0.132	1.155	20	62	2	Apollo
2014 WU200	29.1	1.3	0.071	1.028	7	46	1	Apollo
2014 WX202	29.6	0.4	0.059	1.036	6	41	1	Apollo

2014 WA366	26.9	1.6	0.071	1.034	20	54	1	Apollo
2014 YD	24.3	1.7	0.087	1.072	20	104	1	Apollo
2015 JD3	25.5	2.7	0.008	1.058	38	37	1	Amor
2015 PS228	28.8	0.4	0.084	1.057	9	38	1	Apollo
2015 VC2	27.4	0.9	0.074	1.053	16	111	2	Apollo
2015 XZ378	27.2	2.7	0.035	1.015	17	35	1	Apollo
2015 YO10	26.6	2.4	0.100	1.122	23	28	1	Apollo
2016 CF137	25.6	2.5	0.100	1.091	36	50	1	Apollo
2016 RD34	27.7	2.0	0.035	1.046	14	90	1	Apollo
2016 TB18	24.8	1.5	0.084	1.077	52	98	1	Apollo
2016 TB57	26.1	0.3	0.123	1.102	29	137	1	Apollo
2017 BN93	25.4	2.1	0.052	1.044	40	15	1	Apollo
2017 FJ3	29.9	1.0	0.118	1.133	5	15	1	Apollo
2017 FT102	29.5	1.5	0.059	1.038	6	79	1	Apollo
2017 HU49	26.5	2.6	0.055	0.971	24	147	1	Aten

Table 3 Selected asteroid flyby and rendezvous missions before 2043 prioritizing flight time and observation time

Asteroid Des. ID	Escape from Earth	Arrival at asteroid	T_{oF} [day]	T_{obs} [day]	Δv_{stop} [m/s]
1991 VG	2038 NOV 29	2041 FEB 23	817	7.9	120.1
2000 LG6	2028 MAY 16	2030 MAY 10	724	0.2	936.9
2000 SG344	2028 MAY 09	2029 JUL 02	418	54.8	44.0
	2028 MAY 10	2030 JUN 20	771	59.2	39.8
2001 GP2	2038 MAR 25	2039 JUL 14	476	1.5	694.2
2005 QP87	2034 AUG 24	2037 JAN 19	879	0.7	770.9
2006 RH120	2028 NOV 14	2029 OCT 01	320	1.5	662.7
2006 UB17	2033 OCT 24	2035 OCT 14	719	1.1	891.0
2007 UN12	2035 OCT 15	2037 NOV 04	752	2.9	138.1
2007 VU6	2037 DEC 15	2039 MAR 01	441	1.0	920.2

2008 EA9	2033 NOV 25	2035 MAR 15	475	2.9	217.8
2008 HU4	2026 APR 25	2027 JUL 29	460	2.3	186.8
	2026 APR 25	2028 OCT 04	893	3.5	94.1
2008 UA202	2028 OCT 20	2030 SEP 22	702	1.3	209.2
2009 BD	2034 JUN 03	2035 MAY 07	338	1.8	258.3
2009 YR	2031 NOV 15	2033 APR 05	507	1.5	535.4
2010 JW34	2039 NOV 05	2042 JUL 27	995	1.1	887.1
2010 UJ	2034 SEP 19	2035 MAY 25	248	3.5	369.9
2010 UE51	2036 NOV 25	2037 OCT 11	320	2.6	390.0
2010 VQ98	2039 NOV 13	2041 OCT 01	688	4.3	198.7
	2039 NOV 08	2042 SEP 05	1032	5.1	87.2
2011 BL45	2028 AUG 15	2029 JUL 01	320	0.8	751.3
2011 BQ50	2037 FEB 02	2038 MAR 09	400	0.8	663.0
2011 MD	2036 JUN 23	2038 SEP 10	809	3.7	134.4
2011 UD21	2039 APR 14	2041 JAN 14	641	0.7	589.8
2012 TF79	2026 APR 09	2027 DEC 01	601	1.7	375.5
	2027 FEB 14	2028 DEC 20	675	1.8	862.8
2012 WR10	2038 OCT 13	2039 MAR 18	156	1.4	667.8
2013 BS45	2024 NOV 15	2026 MAY 16	547	1.5	977.2
2013 EC20	2033 MAY 15	2035 JUN 10	756	0.1	983.0
2013 RZ53	2023 SEP 06	2027 NOV 28	1544	0.3	484.7
2014 DJ80	2038 AUG 14	2040 MAY 04	629	0.9	993.0
2014 HN2	2029 MAR 06	2032 MAR 11	1101	1.3	772.6
2014 QN266	2026 FEB 14	2027 MAY 05	445	1.4	820.8
2014 UV210	2034 NOV 14	2036 MAR 14	486	1.1	783.1
2014 WU200	2039 DEC 17	2040 SEP 17	275	2.8	104.7
2014 WX202	2035 FEB 13	2036 JAN 04	325	1.3	406.0

	2034 NOV 28	2037 MAR 15	838	2.4	100.6
2014 WA366	2033 NOV 28	2034 SEP 25	301	1.3	650.8
2014 YD	2035 APR 30	2036 FEB 25	301	3.1	967.8
	2024 JAN 18	2027 MAY 25	1223	8.2	348.3
2015 JD3	2039 MAY 04	2040 DEC 24	600	5.3	663.1
2015 PS228	2027 AUG 16	2028 JUN 06	295	0.7	475.0
2015 VC2	2029 MAR 19	2031 JAN 01	653	3.8	188.9
2015 XZ378	2023 MAY 17	2026 OCT 26	1258	0.7	865.3
2015 YO10	2028 JAN 18	2028 NOV 18	306	0.9	957.5
2016 CF137	2040 JAN 31	2040 DEC 02	306	1.9	776.0
2016 RD34	2031 SEP 12	2033 AUG 11	699	6.2	87.4
2016 TB18	2026 MAR 29	2027 FEB 01	309	6.8	309.4
2016 TB57	2024 JAN 20	2025 JAN 21	367	2.3	542.5
2017 BN93	2032 AUG 14	2033 NOV 21	464	7.2	725.4
2017 FJ3	2034 MAR 04	2035 JUN 02	455	0.3	831.3
2017 FT102	2034 SEP 29	2035 JUN 13	257	0.3	863.0
2017 HU49	2039 MAY 15	2040 MAR 05	295	3.6	669.4

As for asteroid sample return and retrieval, 25 targets are found to be possible by 2043. Each can be retrieved with a Sun-driven lunar swingby sequence and a $\Delta v_{\text{retn}} < 500$ m/s. Again, not all feasible mission profiles can be presented, but the representative missions prioritizing Δv_{retn} are presented in Table 5. Readers interested in all mission options may contact the author. All of the retrievable targets are included in the list of easily reachable asteroids, and thus readers can refer to Table 2 for general information on the target. Among the listed missions, Δv_{retn} is particularly small for the 1991 VG mission, which is 32 m/s. Even though 1991 VG is 5 to 10 times heavier than 2006 RH120 and 2008 UA202, the required total impulse to return 1991 VG to the vicinity of the Earth is still the minimum among all listed missions. The mass of the 10-m across 1991 VG is estimated to be 1500 tons (i.e., at an assumed density of 2.8 g/cm³). The required total impulse is 4.6×10^4 kN · s, within the capacity of state-of-the-art heavy-lift boosters [15].

If low-cost asteroid rendezvous is also required, Table 5 presents representative low-cost retrieval missions

Table 4 Selected asteroid sample-return and retrieval missions prioritizing Δv_{retn}

Asteroid	Departure for Earth	Arrive at Earth	Δv_{retn} [m/s]
1991 VG	2036 JAN 07	2038 DEC 03	31.6
2000 SG344	2028 MAR 13	2030 OCT 07	182.9
2006 RH120	2028 APR 13	2028 NOV 12	143.6
2007 UN12	2031 NOV 09	2035 OCT 26	75.8
2008 EA9	2030 FEB 11	2034 FEB 08	70.0
2008 HU4	2033 FEB 22	2037 APR 25	148.7
2008 UA202	2025 DEC 02	2028 OCT 05	161.8
2009 BD	2031 APR 22	2035 JUN 04	142.6
2010 JW34	2038 JUN 03	2041 MAY 10	396.5
2010 UJ	2032 MAY 09	2033 DEC 06	389.6
2010 UE51	2035 JUN 08	2036 NOV 06	131.9
2010 VQ98	2039 FEB 06	2040 NOV 06	65.4
2011 UD21	2038 JUL 25	2041 OCT 11	68.0
2012 TF79	2026 MAR 03	2027 OCT 14	346.4
2014 WU200	2035 JUN 22	2038 DEC 18	104.0
2014 WX202	2030 JUL 26	2033 NOV 24	94.5
2014 WA366	2030 APR 23	2034 JUL 07	489.7
2014 YD	2034 JAN 21	2036 JAN 19	353.2
2015 PS228	2026 APR 23	2029 MAR 11	489.7
2015 VC2	2025 JAN 05	2029 FEB 19	281.2
2016 RD34	2029 SEP 09	2032 SEP 12	151.6
2016 TB18	2032 JUL 27	2036 MAR 19	234.4
2017 BN93	2027 AUG 24	2031 AUG 08	166.7
2017 FJ3	2028 MAR 16	2029 MAR 13	479.9
2017 FT102	2030 SEP 09	2034 APR 19	485.4

for 16 asteroids, prioritizing the total flight time ToF_{tot} in the heliocentric phase. To exemplify, Fig. 9 presents a set of trajectory options for the 1991 VG retrieval mission, and Fig. 10 presents the trajectories for the 2000 SG344 sample-return mission.

Table 5 Selected asteroid sample-return and retrieval missions constrained by gravity-assisted asteroid rendezvous and prioritizing the total flight time

Asteroid	Escape from Earth	Arrival at asteroid	Δv_{stop} [m/s]	Departure for Earth	Δv_{retn} [m/s]	Return to Earth	ToF_{tot} [day]
1991 VG	2031 NOV 29	2035 SEP 18	949	2036 JAN 07	31.6	2038 DEC 03	2561
2000 SG344	2024 FEB 15	2026 JUL 03	730	2027 NOV 07	221.2	2029 APR 06	1877
2006 RH120	2024 JAN 27	2026 OCT 11	828	2027 JUL 08	438.6	2028 OCT 23	1731
2007 UN12	2030 FEB 14	2033 AUG 22	973	2033 SEP 26	149.0	2035 OCT 19	2073
2008 HU4	2024 FEB 15	2027 JUN 22	978	2033 FEB 17	335.6	2036 APR 28	4456
2008 UA202	2024 FEB 15	2026 AUG 04	918	2026 DEC 21	329.2	2028 OCT 05	1694
2009 BD	2024 MAY 16	2026 OCT 14	712	2029 JAN 03	418.2	2033 MAY 23	3294
2010 UJ	2024 OCT 20	2028 JAN 18	638	2029 JUL 29	410.2	2032 DEC 04	2967
2010 UE51	2024 NOV 15	2027 APR 04	784	2031 SEP 04	470.4	2035 NOV 27	4029
2010 VQ98	2029 NOV 14	2033 JUL 20	961	2034 SEP 26	471.9	2037 OCT 29	2905
2011 UD21	2031 APR 17	2035 APR 21	884	2035 NOV 17	398.2	2038 OCT 15	2738
2014 WU200	2031 JUN 18	2035 JAN 03	942	2035 JUN 22	104.0	2038 DEC 18	2740
2012 TF79	2024 FEB 15	2026 DEC 03	839	2039 JAN 27	397.9	2042 OCT 18	6820
2014 WX202	2027 MAY 17	2030 DEC 07	991	2032 SEP 27	273.9	2033 NOV 23	2382
2015 VC2	2025 MAR 27	2029 JAN 14	807	2037 NOV 01	473.5	2041 DEC 31	6123
2016 TB18	2024 MAR 30	2028 APR 09	570	2034 DEC 05	273.1	2036 MAR 24	4377

6 Discussions

6.1 Considerations and applications of transfer options

Figure 11 presents options of gravity-assisted trajectories to capture the sample from 2009 BD arriving in the vicinity of the Earth around 2033 May 15. The upper-left panel demonstrates the capture trajectory adopting a short inner M-M transfer and two Sun-perturbed transfers. The upper-right panel demonstrates another option adopting a three-rev transfer. The inner M-M transfer is not always necessary. Furthermore, it is considered not practical given the short period between two consecutive lunar swingbys and the consequent challenge for navigation. As for the multi-rev M-M transfers, since they regularly pass the orbit of the Moon, they can be perturbed by the gravity of the Moon, which is not described by the “simplified” model used in this work. Hence, the designed trajectory involving multi-rev M-M transfers cannot be used directly without

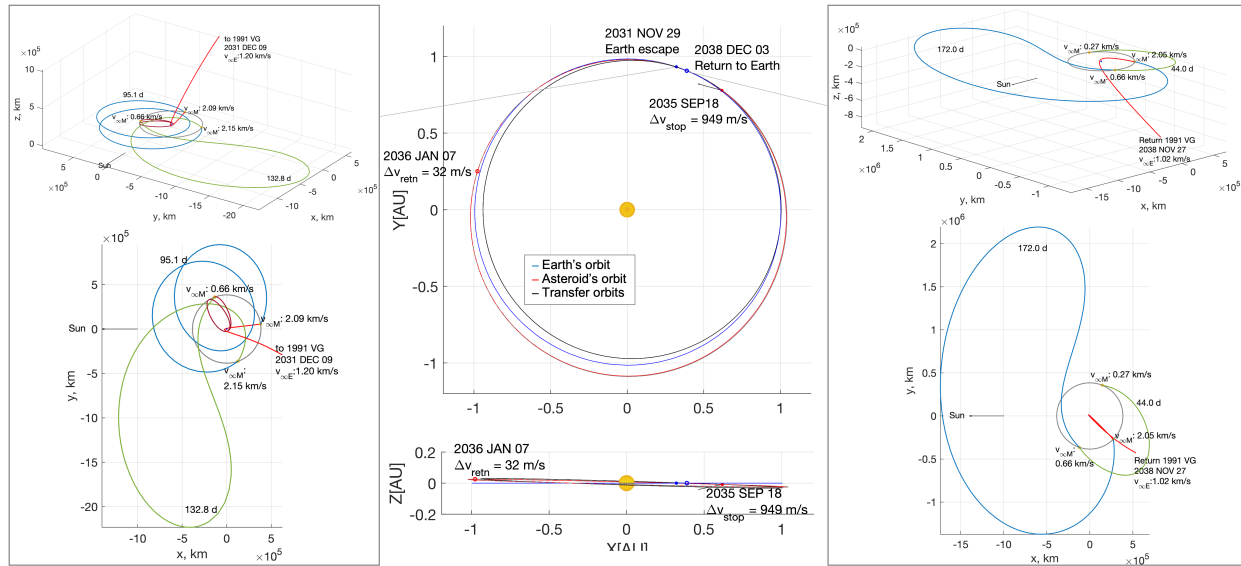


Fig. 9 An example 1991 VG retrieval mission profile, with a gravity-assisted escape phase (left), the heliocentric transfer phase for asteroid rendezvous and Earth re-encounter (middle), and a gravity-assisted capture phase (right).

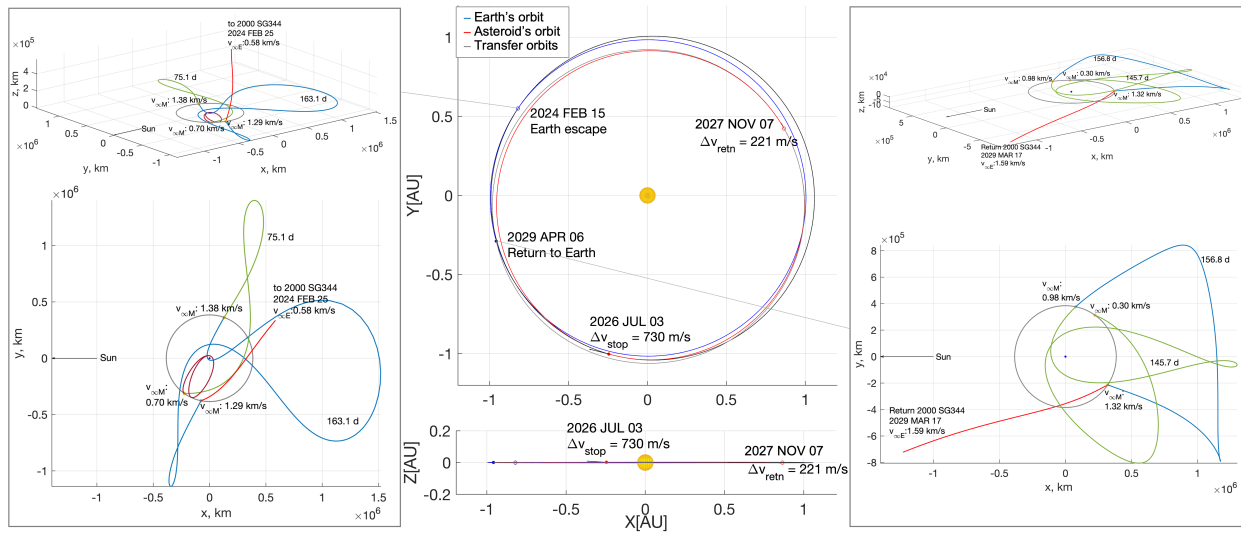


Fig. 10 An example 2000 SG344 sample-return mission profile, with a gravity-assisted escape phase (left), the heliocentric transfer phase for asteroid rendezvous and Earth re-encounter (middle), and a gravity-assisted capture phase (right).

further refinement in the high-fidelity model. Nevertheless, the simplified model provides insights into orbit dynamics and handy approaches to orbit design, which are tricky in the high-fidelity model. A number of transfer options generated by this method can serve as the initial conditions for orbit optimization in

the high-fidelity model. The trajectory refinement and optimization may result in a few small Δv during the courses of M-M transfers, which is to either avoid or make use of the gravity of the Moon. Lantoine and McElrath (2014) [34] have demonstrated that the Sun-driven lunar swingby sequence designed in the simplified model can be successfully transferred to the ephemeris model without significant correction.

In addition, options without the short inner transfer or the multi-rev transfer may be available. The bottom two panels present the trajectory options for different first lunar phase angles (or the Earth encounter dates). In the bottom-left panel, the retrograde transfer arc is greatly decelerated around the apogees in the 2nd quadrant, and the orbit finally becomes a posigrade orbit with a small $v_{\infty M}$. However, the two SPMTs take as long as 200 days. The bottom-right panel demonstrates a more favorable option, where only one large M-M transfer arc and one lunar swingby are needed, which causes minimum flight time (i.e., 120 days) and GNC challenge. To sum up, it is advantageous to have a complete database of SPMT (e.g., including multi-rev transfers) and fully explore possible sequences, so as to gain flexibility and robustness with backup options.

6.2 Three-dimensional Moon-to-Moon transfers

The three-dimensional (3D) SPMT also exists and can serve to connect two lunar encounters. A database of 3D transfers has also been computed using a similar routine as that presented in Sec. 4.2.1. Example 3D trajectories (i.e., $v_{\infty M} = 1.2$ km/s; “oo 1:2” family) are shown in Fig. 12. Observation of the 3D solutions shows that $v_{\infty M}$ at the lunar encounters are generally large (i.e., > 0.8 km/s). That is because the out-of-plane component of $\mathbf{v}_{\infty M}$ cannot be significantly varied by solar tides. The 3D transfer can change the connecting phase, like a non-perturbed lunar resonant orbit can do, and thus add more patching options. Nevertheless, it is considered not efficient especially for the concerned problem where ToF and segments of perturbed M-M transfers are limited. Therefore, for the escape phase, it is preferred to perform the sequence of planar M-M transfers and lunar swingbys before the final bend to the out-of-plane trajectory heading for the asteroid. Similarly, for the capture phase, it is preferred to first bend the out-of-plane incident trajectory to the plane for the following effective gravity assists performed in the plane.

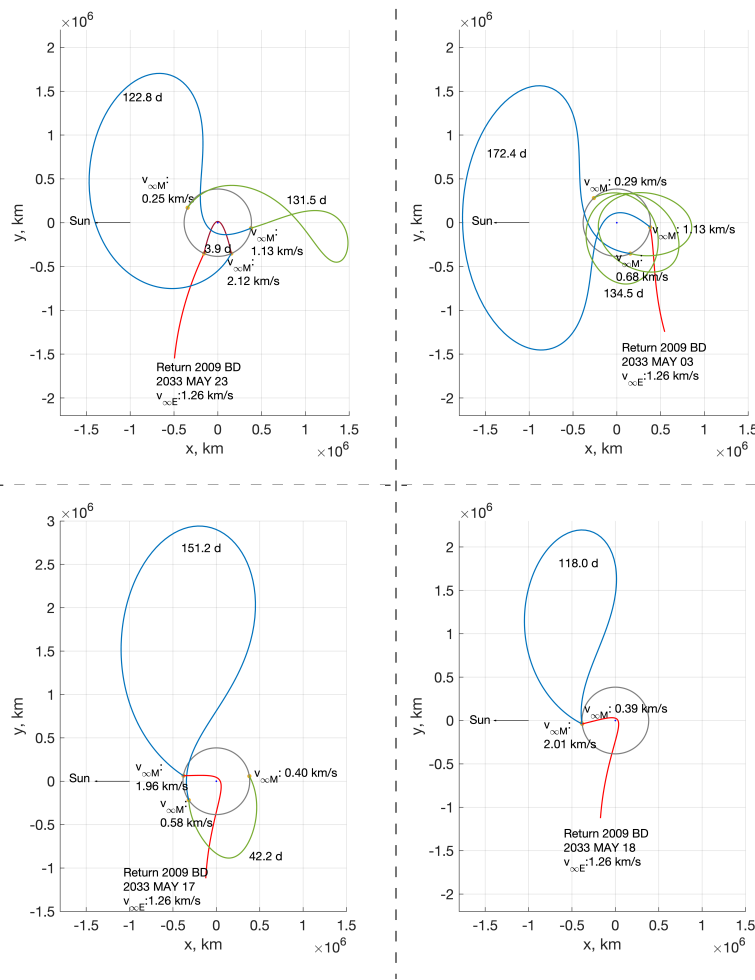


Fig. 11 Available options of lunar swingby sequence for capturing the 2009 BD sample arriving around 2033 May 15 (synodic frame).

7 Conclusions

This paper presents the capacity and application of the Sun-driven lunar swingby sequence. A variety of types of Moon-to-Moon transfer, namely the short transfer, Sun-perturbed transfer, multi-rev transfer, and three-dimensional transfer, were discussed. Analyses with the “Swingby-Jacobi” graph indicate that

- (1) A Sun-driven lunar swingby sequence can access a range of Jacobi integral from -3.0009 to -2.9946.

This range encloses 657 potential asteroids currently cataloged, which can reduce the effort of target search and trajectory optimization.

- (2) C_3 for escape can be increased to $4.8 \text{ km}^2/\text{s}^2$. Reversely, objects of this C_3 level can possibly (depending

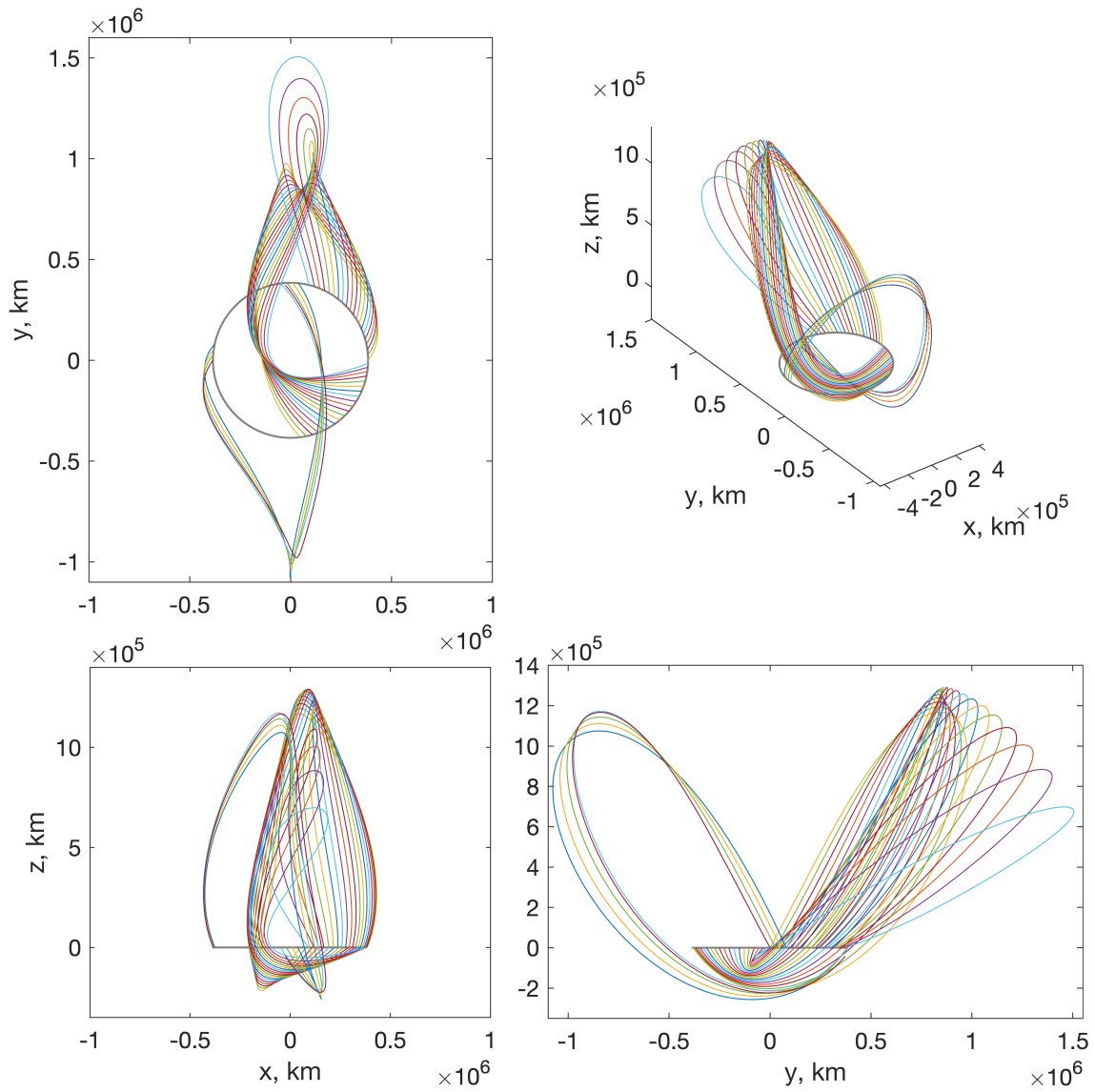


Fig. 12 Example three-dimensional Sun perturbed Moon-to-Moon transfers (synodic frame).

on the direction) be captured. This technique can at least reach or absorb a $v_{\infty E}$ of 1.46 km/s (i.e., C_3 of $2.13 \text{ km}^2/\text{s}^2$) in all directions.

Heliocentric transfer trajectories between the Earth and the potential candidates were optimized, and massive sequences of lunar swingbys were explored thanks to the database of Sun-perturbed Moon-to-Moon transfers. Results shows that Sun-driven lunar swingby sequences can enable:

- (3) spacecraft to rendezvous with 48 asteroids easily by 2043, at a Δv cost less than 1 km/s after the first lunar encounter. Even without the rendezvous Δv , spacecraft can still flyby and observe the asteroids, such as 1991 VG, 2000 SG344, 2014 YD, 2016 TB18, and 2017 BN93, for more than one week. This is still significant for a low-cost mission.
- (4) 25 asteroid samples to be captured by 2043, at a Δv cost less than 500 m/s for Earth re-encounter (while lunar orbit injection requires an additional 20 to 350 m/s of Δv). In particular, given the capabilities of state-of-the-art launch and propulsion systems, the retrieval of the entire 10-m dimension asteroid 1991 VG in 2038, which requires a total impulse of 4.6×10^4 kN · s, is considered feasible.

Appendix (Patching the heliocentric phase and the lunar swingby sequence)

Considering the capture case, given incident $\mathbf{v}_{\infty E}$ and Moon's position vector \mathbf{r}_M as the encounter conditions, the orbital elements of the hyperbolic orbit with respect to the Earth can be computed with the routine presented in this appendix. There are two situations of encountering. One kind of encounter takes place on the inbound leg, and another kind of encounter takes place on the outbound leg (see Fig. 13). For the inbound-capture case, the relationship between true anomaly f at the encounter, turn angle ζ (i.e., half the bending angle), and the angle β between $\mathbf{v}_{\infty E}$ and \mathbf{r}_M is expressed by,

$$\cos f = \cos(\beta - \zeta) \quad (13)$$

which can be rewritten as,

$$\cos f = \sin \beta \sin \zeta + \cos \beta \cos \zeta \quad (14)$$

ζ is related to eccentricity e_p of the orbit with respect to the Earth. Hence,

$$\cos f = \frac{\sqrt{e_p^2 - 1}}{e_p} \sin \beta + \frac{1}{e_p} \cos \beta \quad (15)$$

At the encounter, the radius of the hyperbolic orbit of semi-major axis a with respect to the Earth is the same as the radius of the Moon's orbit, which is expressed as,

$$r_M = \frac{a_p(1 - e_p^2)}{1 + e_p \cos f} \quad (16)$$

where the semi-major axis a_p is related to $v_{\infty E}$ through,

$$a_p = -G_E / v_{\infty E}^2 \quad (17)$$

where G_E is the gravitational parameter of the Earth. Integrating the last two equations yields a quadratic function of $\sqrt{e_p^2 - 1}$,

$$a_p(e_p^2 - 1) + r_M \sin \beta \sqrt{e_p^2 - 1} + r_M(1 + \cos \beta) = 0 \quad (18)$$

whose solution is computed from,

$$\sqrt{e_p^2 - 1} = \frac{-r_M \sin \beta - \sqrt{r_M^2 \sin^2 \beta - 4a_p r_M(1 + \cos \beta)}}{2a_p} \quad (19)$$

With e_p known, the orbit is determined. The true anomaly is computed from,

$$f = -\arccos[(a_p(1 - e_p^2) - r_M)/r_M/e_p] \quad (20)$$

Other desired information at the lunar encounter can be derived. The steps of deriving the e_p and f for the outbound-capture, inbound-escape, and outbound-capture cases are similar. The corresponding expressions are directly given as follows. For the outbound-capture case,

$$\sqrt{e_p^2 - 1} = \frac{r_M \sin \beta - \sqrt{r_M^2 \sin^2 \beta - 4a_p r_M(1 + \cos \beta)}}{2a_p} \quad (21)$$

$$f = \arccos[(a_p(1 - e_p^2) - r_M)/r_M/e_p] \quad (22)$$

For the inbound-escape case,

$$\sqrt{e_p^2 - 1} = \frac{r_M \sin \beta - \sqrt{r_M^2 \sin^2 \beta - 4a_p r_M(1 - \cos \beta)}}{2a_p} \quad (23)$$

$$f = -\arccos[(a_p(1 - e_p^2) - r_M)/r_M/e_p] \quad (24)$$

For the outbound-escape case,

$$\sqrt{e_p^2 - 1} = -\frac{r_M \sin \beta + \sqrt{r_M^2 \sin^2 \beta - 4a_p r_M(1 - \cos \beta)}}{2a_p} \quad (25)$$

$$f = \arccos[(a_p(1 - e_p^2) - r_M)/r_M/e_p] \quad (26)$$

Acknowledgements

This work was primarily conducted at the Engineering and Technology Center for Space Utilization, Chinese Academy of Sciences. The massive exploration of sequences of Moon-to-Moon transfers and lunar swingbys benefited from the computer cluster *cerfeuil*, financed and managed by IMCCE/Paris Observatory. The author sincerely appreciates the valuable comments from the anonymous reviewers.

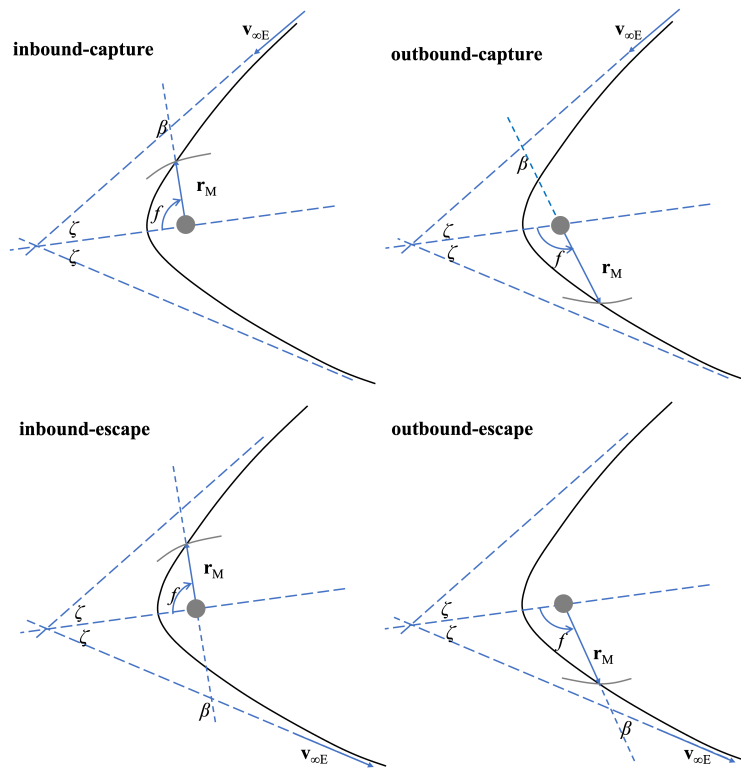


Fig. 13 Situations of lunar encounters with a hyperbolic orbit on the inbound leg and outbound leg.

Declaration of competing interest

The authors have no competing interests to declare that are relevant to the content of this article.

References

- [1] Uesugi K, Matsuo H, Kawaguchi J, Hayashi T. Japanese first double lunar swingby mission “Hiten”. *Acta Astronautica*, 1991, 25(7): 347–355, doi:10.1016/0094-5765(91)90014-V.
- [2] Folta DC, Woodard M, Howell K, Patterson C, Schlei W. Applications of multi-body dynamical environments: The ARTEMIS transfer trajectory design. *Acta Astronautica*, 2012, 73: 237–249, doi: 10.1016/j.actaastro.2011.11.007.
- [3] Kawaguchi J, Nakatani I, Uesugi T, Tsuruda K. Synthesis of an alternative flight trajectory for Mars explorer, Nozomi. *Acta Astronautica*, 2003, 52(2): 189–195, doi:10.1016/S0094-5765(02)00156-X, selected Proceedings of the 4th IAA International conference on Low Cost Planetary Missions.

- [4] Chen H. NEW RESULTS OF ORBITAL DYNAMICS AND THE APPLICATION TO ORBIT PREDICTION AND MISSION DESIGN. Phd thesis, Kyushu University, 2015, doi:10.15017/1543984, 63-157.
- [5] Chen H, Kawakatsu Y, Hanada T. Earth Escape from a Sun-Earth Halo Orbit using Unstable Manifold and Lunar Swingbys. *Transactions of the Japan Society for Aeronautical and Space Sciences*, 2016, 59(5): 269–277, doi:10.2322/tjsass.59.269.
- [6] Garcia Yárnoz D, Yam CH, Campagnola S, Kawakatsu Y. EXTENDED TISSERAND-POINCARÉ GRAPH AND MULTIPLE LUNAR SWINGBY DESIGN WITH SUN PERTURBATION. In *6th International Conference on Astrodynamics Tools and Techniques*, Darmstadt, Germany 2016.
- [7] Grebow D, Campagnola S, Haw R, Sweeter T. Lunar Flashlight Mission Overview. In *Inter-planetary Small Satellite Conference*, Pasadena, CA, USA 2020.
- [8] Cheng AF, Rivkin AS, Michel P, Atchison J, Barnouin O, Benner L, Chabot NL, Ernst C, Fahnestock EG, Kueppers M, Pravec P, Rainey E, Richardson DC, Stickle AM, Thomas C. AIDA DART asteroid deflection test: Planetary defense and science objectives. *Planetary and Space Science*, 2018, 157: 104–115, doi:10.1016/j.pss.2018.02.015.
- [9] Michel P, Küppers M, Bagatin AC, Carry B, Charnoz S, de Leon J, Fitzsimmons A, Gordo P, Green SF, Hérique A, Juzi M, Özgür Karatekin, Kohout T, Lazzarin M, Murdoch N, Okada T, Palomba E, Pravec P, Snodgrass C, Tortora P, Tsiganis K, Ulamec S, Vincent JB, Wünnemann K, Zhang Y, Raducan SD, Dotto E, Chabot N, Cheng AF, Rivkin A, Barnouin O, Ernst C, Stickle A, Richardson DC, Thomas C, Arakawa M, Mioto H, Nakamura A, Sugita S, Yoshikawa M, Abell P, Asphaug E, Ballouz RL, Bottke WF, Lauretta DS, Walsh KJ, Martino P, Carnelli I. The ESA Hera Mission: Detailed Characterization of the DART Impact Outcome and of the Binary Asteroid (65803) Didymos. *The Planetary Science Journal*, 2022, 3(7): 160, doi:10.3847/PSJ/ac6f52.
- [10] Brophy J, Culick F, Friedman L, Allen C, Baughman D, Bellerose J, Betts B, Brown M, Busch M, Casani J, Coradini M, Dankanich J, Dimotakis P, Elvis M, Garrick-Bethel I, Gershman B, Jones T, Landau D, Lewicki C, Lewis J, Llanos P, Lupisella M, Mazanek D, Mehrotra P, Nuth J, Parkin K, Schweickart R, Singh G, Strange N, Tantardini M, Wilcox B, Williams C, Williams W, Yeomans D. Technical report, Keck Institute for Space Studies, California Institute of Technology, Jet Propulsion Laboratory, Pasadena, California, 2012.

- [11] Baoyin HX, Chen Y, Li JF. Capturing near earth objects. *Research in Astronomy and Astrophysics*, 2010, 10(6): 587, doi:10.1088/1674-4527/10/6/008.
- [12] Sanchez Cuartielles JP, Garcia Yarnoz D, Alessi E, McInnes C. Gravitational capture opportunities for asteroid retrieval missions. In *Proceedings of 63rd International Astronautical Congress*, Naples, Italy 2012.
- [13] Lladó N, Ren Y, Masdemont JJ, Gómez G. Capturing small asteroids into a Sun–Earth Lagrangian point. *Acta Astronautica*, 2014, 95: 176–188, doi:10.1016/j.actaastro.2013.11.007.
- [14] Sanchez JP, Garcia Yáñez D. Asteroid retrieval missions enabled by invariant manifold dynamics. *Acta Astronautica*, 2016, doi:10.1016/j.actaastro.2016.05.034.
- [15] Landau D, Dankanich J, Strange N, Bellerose J, Llanos P, Tantardini M. Trajectories to NAB a NEA (near-Earth asteroid). *Advances in the Astronautical Sciences*, 2013, 148(February): 3251–3262.
- [16] Gong S, Li J. Asteroid capture using lunar flyby. *Advances in Space Research*, 2015, 56(5): 848–858, doi:10.1016/j.asr.2015.05.020.
- [17] Urrutxua H, Scheeres DJ, Bombardelli C, Gonzalo JL, Peláez J. Temporarily Captured Asteroids as a Pathway to Affordable Asteroid Retrieval Missions. *Journal of Guidance, Control, and Dynamics*, 2015, 38(11): 2132–2145, doi:10.2514/1.G000885.
- [18] Mingotti G, Topputo F, Bernelli-Zazzera F. Optimal low-thrust invariant manifold trajectories via attainable sets. *Journal of Guidance, Control, and Dynamics*, 2011, 34(6): 1644–1655, doi:10.2514/1.52493.
- [19] Chilan CM, Conway Ba. A Reachable Set Analysis Method for Generating Near-Optimal Trajectories of Constrained Multiphase Systems. *Journal of Optimization Theory and Applications*, 2014, 167: 161–194, doi:10.1007/s10957-014-0651-2.
- [20] Bando M, Scheeres DJ. Attractive Sets to Unstable Orbits Using Optimal Feedback Control. *Journal of Guidance, Control, and Dynamics*, 2016, 39(12): 2725–2739, doi:10.2514/1.G000524.
- [21] Topputo F, Wang Y, Giordano C, Franzese V, Goldberg H, Perez-Lissi F, Walker R. Envelope of reachable asteroids by M-ARGO CubeSat. *Advances in Space Research*, 2021, 67(12): 4193–4221, doi:<https://doi.org/10.1016/j.asr.2021.02.031>.
- [22] Wu CY, Russell R. Reachable Set of Low-Delta-v Trajectories Following a Gravity-Assist Flyby. *Journal of Spacecraft and Rockets*, 2023, doi:10.2514/1.A35464, in press.

- [23] Strange NJ, Longuski JM. Graphical Method for Gravity-Assist Trajectory Design. *Journal of Spacecraft and Rockets*, 2002, 39(1): 9–16, doi:10.2514/2.3800.
- [24] Campagnola S, Russell RP. Endgame Problem Part 2: Multibody Technique and the Tisserand-Poincare Graph. *Journal of Guidance, Control, and Dynamics*, 2010, 33(2): 476–486, doi:10.2514/1.44290.
- [25] Ross SD, Scheeres DJ. Multiple Gravity Assists, Capture, and Escape in the Restricted Three-Body Problem. *SIAM Journal on Applied Dynamical Systems*, 2007, 6(3): 576–596, doi:10.1137/060663374.
- [26] Chen H. THE USE OF LUNI-SOLAR GRAVITY ASSISTS FOR ASTEROID RETRIEVAL. In JW McMahon, FW Leve, Y Guo, Jon, editors, *Advances in the Astronautical Sciences*, volume 160, 2017, 4043–4060, also proceedings of the AAS/AIAA Spaceflight Mechanics Meeting, San Antonio, TX, USA, FEB 05-09, 2017.
- [27] Martens W, Bucci L. Double Tisserand graphs for low-energy lunar transfer design. *Frontiers in Space Technologies*, 2022, 3, doi:10.3389/frspt.2022.920456.
- [28] Oguri K, Oshima K, Campagnola S, Kakihara K, Ozaki N, Baresi N, Kawakatsu Y, Funase R. EQUULEUS Trajectory Design. *The Journal of the Astronautical Sciences*, 2020, 67(3): 950–976, doi:10.1007/s40295-019-00206-y.
- [29] Thompson M, Kayser E, Parker J, Ott C, Bolliger M, Gardner T, Cheetham B. Navigation Design of the CAPSTONE Mission Near NRHO Insertion. In *AAS/AIAA Astrodynamics Specialist Conference*, Big Sky, MT, USA2021.
- [30] Curtis HD. Chapter 8 - Interplanetary Trajectories. In HD Curtis, editor, *Orbital Mechanics for Engineering Students (Third Edition)*, third edition edition, Boston: Butterworth-Heinemann2014, 405–457, doi:<https://doi.org/10.1016/B978-0-08-097747-8.00008-6>.
- [31] Kemble S. *Interplanetary Mission Analysis and Design*, chapter Special techniques, Berlin, Heidelberg: Springer Berlin Heidelberg2006, 135–333, doi:10.1007/3-540-37645-3_4.
- [32] McElrath TP, Lantoine G, Landau D, Grebow D, Strange N, Wilson R, Sims J. Using gravity assists in the Earth-Moon system as a gateway to the solar system. In *Global Space Exploration Conference*, Washington, D. C., USA: Pasadena, CA : JPL, NASA2012.
- [33] Battin RH. *An Introduction to the Mathematics and Methods of Astrodynamics*. Rev. ed. edition, Reston, Virginia: American Institute of Aeronautics and Astronautics, Inc.1999, doi:10.2514/4.861543.
- [34] Lantoine G, McElrath TP. FAMILIES OF SOLAR-PERTURBED MOON-TO-MOON TRANSFERS.

In *AAS/AIAA Space Flight Mechanics Meeting*, Santa Fe, USA2014.

- [35] Dymock R. The H and G magnitude system for asteroids. *Journal of the British Astronomical Association*, 2007, 117: 342–343.
- [36] Yam C, Sugimoto Y, Ozaki N, Sarli B, Chen H, Campagnola S, Ogura S, Kawabata Y, Kawakatsu Y, Nakajima S, Funase R, Nakasuka S. Launch window and sensitivity analysis of an asteroid flyby mission with miniature ion propulsion system: PROCYON. In *Proceedings of the International Astronautical Congress, IAC*, volume 8, Toronto, Canada2014, 5383 – 5389.

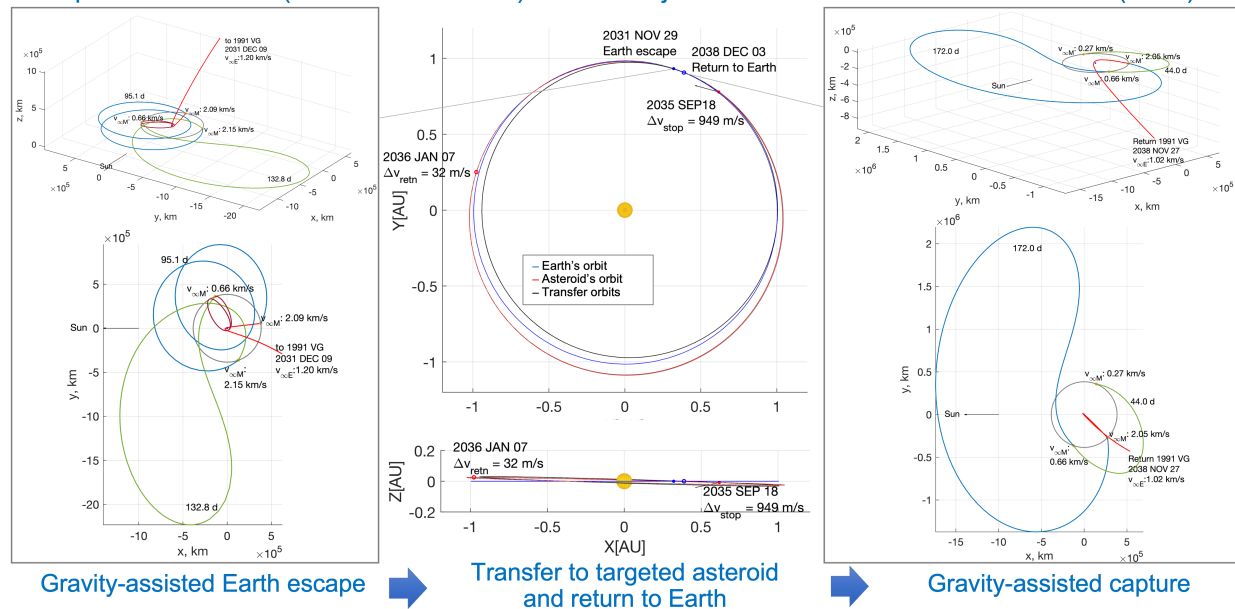
Author biography



Hongru Chen is an Assistant Professor at Kyushu University, Japan. She received her Bachelor's degree from Northwestern Polytechnical University, China, in 2010, and her Ph.D. from Kyushu University, in 2015, both in aerospace engineering. She did her Ph.D. thesis at ISAS/JAXA, once worked at the Chinese Academy of Sciences and IMCCE/Paris Observatory, and participated in JAXA and CNES planetary projects, such as PROCYON, DESTINY, and MMX. Her research interests include astrodynamics, orbit design, nano-satellite engineering, and atmosphere modeling.

Graphical table of contents

A possible mission (02/2031 – 08/2038) and the trajectories to retrieve asteroid 1991 VG (10 m)



1) Capacity of lunar and solar gravity assists for deep-space mission design is characterized. 2) The trajectory design technique is applied to asteroid flyby, rendezvous, sample return, and retrieval. 3) Various Moon-to-Moon transfer types, namely, the short transfer, Sun-perturbed transfer, multi-revolution transfer, and three-dimensional transfer, are covered.

Fig. 14 Graphical abstract of the paper